TITLE

Antinociceptive modulation by the adhesion-GPCR CIRL promotes mechanosensory signal discrimination

AUTHORS

Sven Dannhäuser[1,2], Thomas J. Lux[3], Chun Hu[4], Mareike Selcho[1,2], Jeremy Tsung-Chieh Chen[3], Nadine Ehmann[1,2], Divya Sachidanandan[1,2], Matthias Pawlak[5], Tobias Langenhan[6], Peter Soba[4], Heike Rittner[3], Robert J. Kittel[1,2]

AFFILIATIONS

[1] Department of Animal Physiology, Institute of Biology, Leipzig University, Talstraße 33, 04103 Leipzig, Germany

[2] Carl-Ludwig-Institute for Physiology, Leipzig University, Liebigstraße 27, 04103 Leipzig, Germany

[3] Center for Interdisciplinary Pain Medicine, Department of Anaesthesiology, University Hospital Würzburg, 97080 Würzburg, Germany

[4] Neuronal Patterning and Connectivity, Center for Molecular Neurobiology, University Medical Center Hamburg-Eppendorf, 20251 Hamburg, Germany

[5] Department of Neurophysiology, Institute of Physiology, University of Würzburg, 97080 Würzburg, Germany

[6] Rudolf Schönheimer Institute of Biochemistry, Division of General Biochemistry, Medical Faculty, Leipzig University, Leipzig, Germany

Correspondence and material requests should be addressed to H.R. (Rittner_H@ukw.de) or R.J.K. (rjkittel@me.com)

ABSTRACT

Adhesion-type G protein-coupled receptors (aGPCRs) participate in a vast range of physiological processes. Correspondingly, these receptors are associated with diverse human diseases, such as developmental disorders, defects of the nervous system, allergies and cancer. Several aGPCRs have recently been linked to mechanosensitive functions suggesting that processing of mechanical stimuli may be a common feature of this receptor family. CIRL (ADGRL/Latrophilin, LPHN), one of the oldest members of the aGPCR family, sensitizes sensory responses of larval *Drosophila* to gentle touch and sound by amplifying mechanosensory signal transduction in low-threshold mechanoreceptors (Scholz et al., 2015; 2017). In the present study, we show that *Cirl* is also expressed in high-threshold mechanical nociceptors where it adjusts nocifensive behaviour under physiological and pathophysiological conditions. Optogenetic *in vivo* experiments indicate that CIRL quenches cAMP levels in both mechanosensory submodalities. However, contrasting its effect in touch sensitive neurons, CIRL dampens the response of nociceptors to mechanical stimulation. Consistent with this finding, rat nociceptors display a drop in *Cirl1* expression during allodynia. Taken together, these results demonstrate that CIRL exerts opposing modulatory functions in low-threshold mechanosensors and high-threshold nociceptors. This intriguing bipolar action likely facilitates the separation of mechanosensory signals carrying different physiological information.

INTRODUCTION

Mechanical forces are detected and processed by the somatosensory system. Mechanosensation encompasses the distinct submodalities of touch, proprioception, and mechanical nociception. Touch plays an important discriminative role and contributes to social interactions (Abraira and Ginty, 2013; McGlone et al., 2014). Nociception reports incipient or potential tissue damage. It triggers protective behaviours and can give rise to pain sensations (Basbaum et al., 2009). Thus, physically similar signals can carry fundamentally different physiological information, depending on stimulus intensity. Whereas innocuous touch sensations rely on low-threshold mechanosensory neurons, noxious mechanical stimuli activate high-threshold mechanosensory neurons, i.e. nociceptors. While mechanisms to differentiate these mechanosensory submodalities are essential for survival, little is known how this is achieved at cellular and molecular levels.

The activity of nociceptors can be increased through sensitization, e.g. upon inflammation, and decreased through antinociceptive processes, leading to pain relief. In both cases, G protein-coupled receptors (GPCRs) play an important modulatory role. Receptors that couple to heterotrimeric $G_{q/11}$ or G_s proteins, like the prostaglandin EP_2 receptor, increase the excitability of nociceptors by activating phospholipase C and adenylate cyclase pathways, respectively. In contrast, $G_{i/o}$-coupled receptors, which are gated by soluble ligands like morphine and endogenous opioid neuropeptides generally inhibit nociceptor signaling. In mammalian nociceptors, cell surface receptors that couple to $G_{i/o}$ proteins are located at presynaptic sites in the dorsal horn of the spinal cord, where they reduce glutamate release, at somata in dorsal root ganglia (DRG), and at peripheral processes, where they suppress receptor potential generation (Yudin and Rohacs, 2018).

Research on mechanosensation has focussed mainly on receptors that transduce mechanical force into electrical current, and the function of such mechanosensing ion channels is currently the subject of detailed investigations. In contrast, evidence for mechano-metabotropic signal

transfer and compelling models of force conversion into an intracellular second messenger response are limited, despite the vital role of metabotropic modulation in all corners of physiology (Mederos y Schnitzler et al., 2008; Hoffman et al., 2011). Adhesion-type GPCRs (aGPCRs), a large molecule family with over 30 members in humans, operate in diverse physiological settings (Hamann et al., 2015; Scholz et al., 2016). In contrast to most members of the GPCR phylum, aGPCRs are not activated by soluble ligands. Instead, aGPCRs interact with partner molecules tethered to membranes or fixed to the extracellular matrix via their long, adhesive N-terminal domain. This arrangement positions aGPCRs as metabotropic mechanosensors, which translate a relative displacement of the receptor-bearing cell into an intracellular second messenger signal (Langenhan et al., 2016).

Drosophila CIRL (ADGRL/Latrophilin, Lphn) is expressed in the neuronal dendrites and cilia of larval chordotonal organs (ChOs), mechanosensory structures that respond to gentle touch, sound, and proprioceptive input (Kernan, 2007; Scholz et al., 2015). Mechanical stimulation of CIRL triggers a conformational change of the protein and activation via its tethered agonist (*Stachel*) (Liebscher et al., 2014; Stoveken et al., 2015). Signalling by the activated receptor reduces intracellular cAMP levels, which in turn sensitizes ChO neurons and potentiates the mechanically-evoked receptor potential (Scholz et al., 2017). In the current study, we show that CIRL also adjusts the activity of nociceptors, which respond to strong mechanical stimuli. Here, too, its function is consistent with $G_{i/o}$ coupling. However, in contrast to touch-sensitive ChO neurons, nociceptors are sensitized by elevated cAMP concentrations and toned down by the antinociceptive action of CIRL. As a result, CIRL modulates neural processing of noxious harsh and innocuous gentle touch bidirectionally. This elegant signalling logic serves signal discrimination by helping to separate mechanosensory submodalities.

RESULTS

Drosophila larvae possess two major types of peripheral sensory neurons. Monociliated type 1 neurons, including ChOs and external sensory organs, and type 2 neurons with multiple dendritic (md) projections, classified as tracheal dendrite (md-td), bipolar dendrite (md-bd), and dendritic arborization (md-da). Md-da neurons are further subdivided into four classes: C1da-C4da (Ghysen et al., 1986; Bodmer and Jan, 1987; Grueber et al., 2002). Previous work demonstrated prominent expression of *Cirl* in ChOs, where it modulates sensory processing of innocuous mechanical stimuli (Scholz et al., 2015, 2017). In addition, *Cirl* transcription was also noted in md neurons. Motivated by this observation, we now turned our attention to C4da neurons: polymodal nociceptors, which respond to noxious temperatures, intense light and, importantly, harsh mechanical touch (Tracey et al., 2003; Xiang et al., 2010; Zhong et al., 2010, 2012; Kim et al., 2012; Kim and Johnson, 2014). Degenerin/epithelial sodium channels (DEG/ENaCs) contribute to nociceptive mechanotransduction in invertebrates and mammals (Price et al., 2001; Chatzigeorgiou et al., 2010; Zhong et al., 2010; Gorczyca et al., 2014; Guo et al., 2014; Mauthner et al., 2014). Placing a fluorescent reporter under transcriptional control of the DEG/ENaC subunit *pickpocket* (*ppk*) reliably marks C4da neurons (Grueber et al., 2003; Han et al., 2011). We therefore combined a direct *GFP-ppk* promoter fusion (*ppk-CD4::tdGFP*) with binary expression of the red photoprotein *Tomato* by a *Cirl* promoter element in the *UAS/GAL4* system (*dCirlp^{GAL4} > UAS-CD4::tdTomato*) (Brand and Perrimon, 1993; Scholz et al., 2015). This setting revealed *Cirl* transcription in both *ppk*-negative ChOs and *ppk*-positive C4da neurons (Figure 1). Thus, *Cirl* is expressed in different sensory neurons, including proprioceptors and nociceptors.

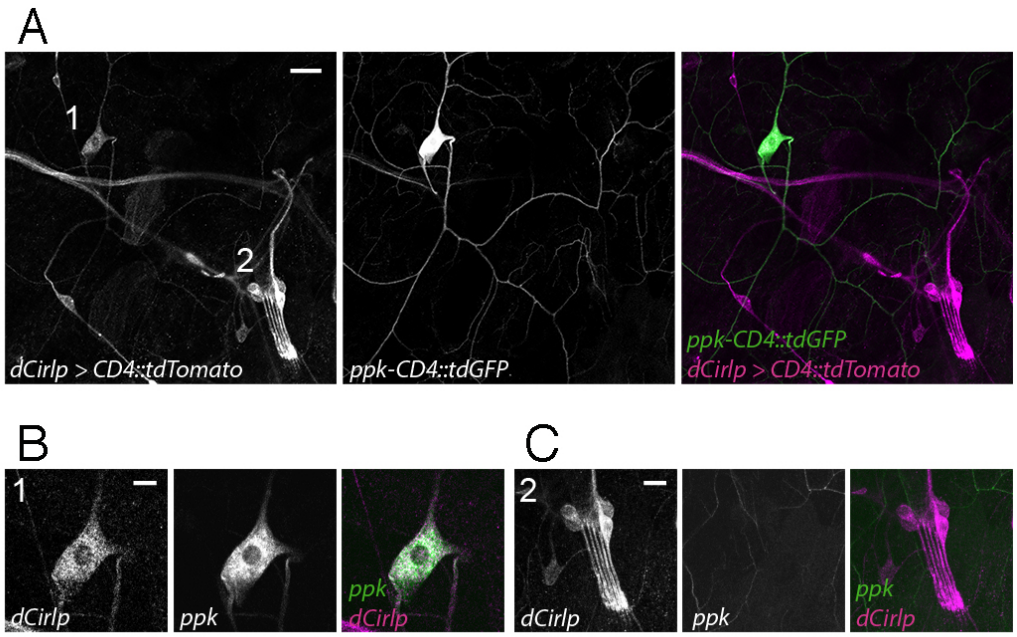

Figure 1. *Drosophila Cirl* is expressed in proprioceptors and nociceptors.
(A) The *Cirl* promoter drives *Tomato* photoprotein expression (magenta; *dCirlp*^{GAL4} > *UAS-CD4::tdTomato*) in type 1 larval pentascolopidial ChO (lch5) neurons and type 2 C4da nociceptors, identified by a *GFP-ppk* promoter fusion (green; *ppk-CD4::tdGFP*). Magnified view of **(B)** C4da and **(C)** ChO neurons. Shown are immunohistochemical stainings against the photoproteins. Scale bars (A) 20 µm, (B,C) 10 µm.

Given CIRL's role in mechanosensation, we next tested for a specific contribution of the aGPCR to mechanical nociception. *Drosophila* larvae display a stereotyped response to noxious mechanical insult. Importantly, this innate nocifensive behaviour, characterized by a "corkscrew" body roll, can be quantified and is distinct from the animals' reaction to innocuous touch (Figure 2A; Video 1) (Tracey et al., 2003; Zhong et al., 2010). Mechanical stimulation with a 40 mN von Frey filament triggered nocifensive behaviour in 53% of control larvae. In contrast, *Cirl* null mutants (*dCirl*^{KO}) showed significantly increased nocifensive behaviour and responded in 75% of the trials (Figure 2B; Table 1). Knocking-down *Cirl* levels specifically in C4da neurons via RNA-interference (RNAi; *ppk-GAL4* > *UAS-dCirl*^{RNAi}) delivered a mutant phenocopy and re-expressing *Cirl* in nociceptors rescued the mutant phenotype. Notably, *Cirl* overexpression had the opposite effect resulting in diminished nocifensive responses (Figure 2B; Table 1). These results show that CIRL curtails mechanical nociception by carrying out a cell-autonomous, dose-dependent function in C4da neurons.

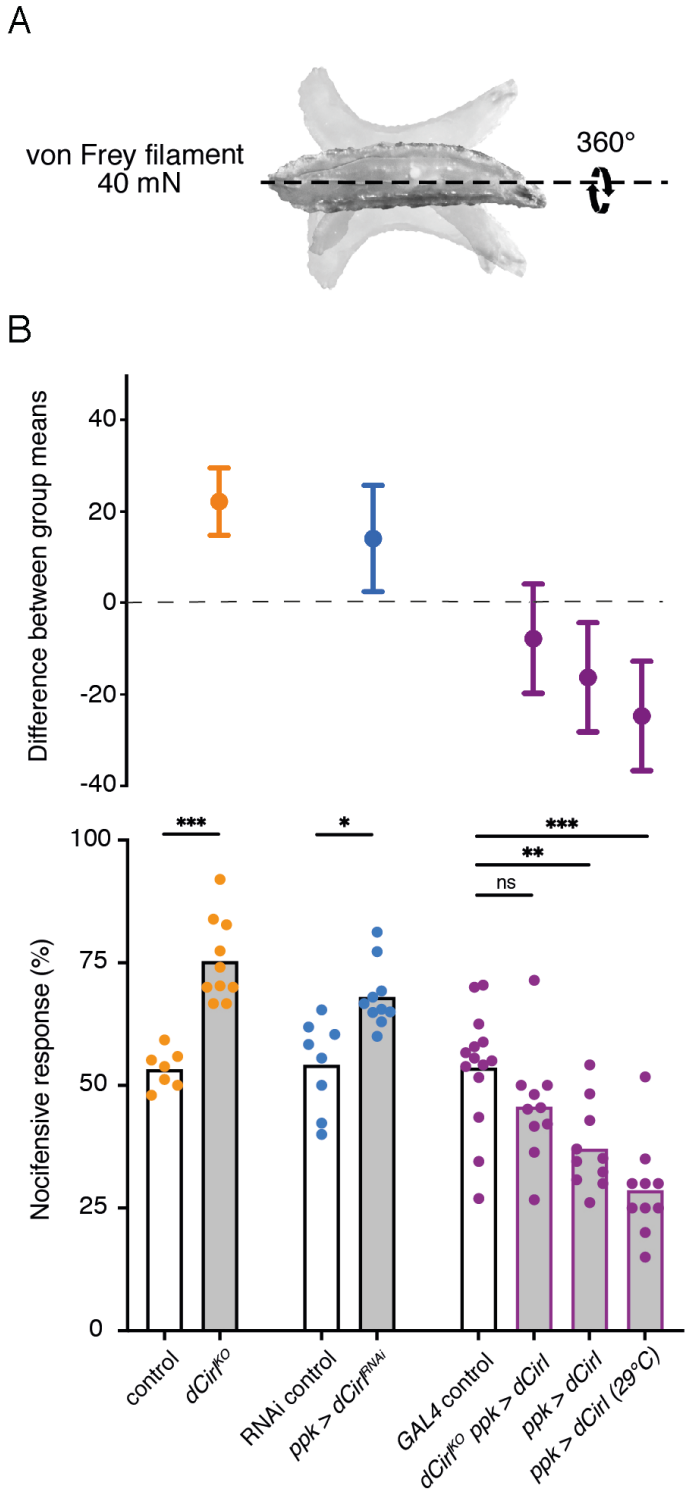

Figure 2. *Cirl* reduces nocifensive behaviour.
(A) Characteristic nocifensive 'corkscrew' roll of larvae upon mechanical stimulation with a von Frey filament (40 mN force). **(B)** Quantification of nocifensive behaviour in different genotypes. Increased nocifensive responses were observed in $dCirl^{KO}$ and upon nociceptor-specific expression of an RNAi construct (*ppk-GAL4* > *UAS-*$dCirl^{RNAi}$). *Cirl* re-expression rescued the null mutant ($dCirl^{KO}$ *ppk-GAL4* > *UAS-dCirl*) and *Cirl* overexpression (*ppk-GAL4* > *UAS-dCirl*) reduced nocifensive responses. Raising animals at a higher temperature (29°C vs. 25°C) increases *UAS/GAL4*-dependent transgene expression (Duffy, 2002). Data are presented as mean and individual values (lower bar plot) and as the difference between means with 95% confidence intervals (upper dot plot). Asterisks denote level of significance, *p ≤ 0.05, **p ≤ 0.01, ***p ≤ 0.001.

CIRL sensitizes proprioceptive ChO neurons by translating extracellular mechanical stimulation into a drop of intracellular cAMP. Lower cAMP levels, in turn, enhance the mechanically-evoked receptor potential of ChOs through a yet unresolved molecular mechanism (Scholz et al., 2017). Intriguingly, our behavioural data point towards CIRL exerting the opposite influence on nociceptive C4da neurons, whose sensitivity to mechanical stimulation is decreased by CIRL and increased in the absence of the aGPCR. A possible explanation for the antinociceptive action of CIRL is that the aGPCR also quenches cAMP in nociceptors, but that here the second messenger cascade acts on different molecular targets, i.e. specific ion channels, to produce an inverted effect. According to this model, low cAMP levels would dampen nociceptor activity. Next, we therefore asked whether increasing cAMP in C4da neurons (as may occur in *dCirl*^{KO}) promotes nocifensive behaviour. Because chronic changes of cAMP levels strongly alter neuronal development (Griffith and Budnik, 2006) we selected an optogenetic approach to trigger a rapid, nociceptor-specific increase of cAMP. The bacterial photoactivated adenylyl cyclase bPAC can be genetically expressed in selected *Drosophila* neurons to evoke cAMP production upon blue light stimulation (Figure 3A) (Stierl et al., 2011; Scholz et al., 2017). Indeed, driving bPAC in C4da neurons (*ppk-GAL4* > *UAS-bPAC*) led to increased nocifensive behaviour during light exposure, whereas control animals showed no light-induced effects (Figure 3B; Table 2). Notably, bPAC expression also produced some irregular behaviour in the absence of photostimulation ('spontaneous bending'; Figure 3B), which is likely a result of the enzyme's residual dark activity (Stierl et al., 2011). Nocifensive responses were further enhanced by bPAC in *dCirl*^{KO} larvae (*dCirl*^{KO} *ppk-GAL4* > *UAS-bPAC*), in line with increased cAMP levels in mutant C4da neurons. Independent support for this conclusion was received by analysing larvae carrying mutant alleles of the phosphodiesterase (PDE) *dunce* (Davis and Kiger, 1981). Here, pronounced nocifensive behaviour accompanies chronically elevated cAMP concentrations (Figure 3C; Table 1).

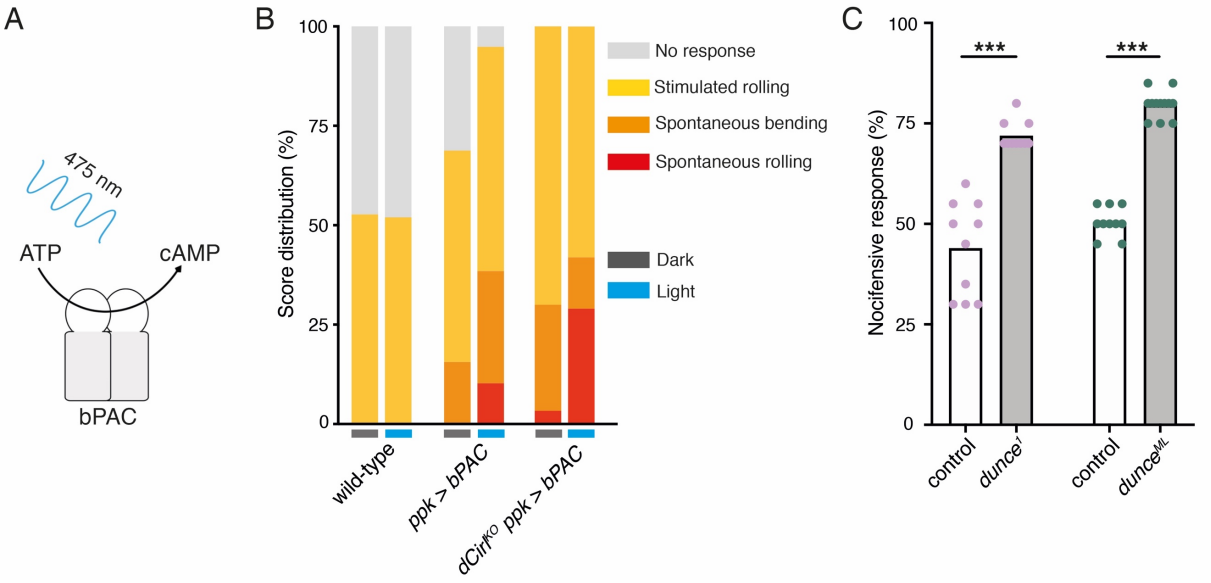

Figure 3. Potentiation of nociceptor function by cAMP.
(A) Schematic illustration of cAMP production by bPAC. **(B)** Optogenetic assay. Stimulated and spontaneous nocifensive responses can be promoted and elicited, respectively, by bPAC activation in C4da neurons (blue labels, photostimulation). Larval behaviour was observed during 3 min illumination (~200 µW/mm^2 at 475 nm) followed by mechanical stimulation (40 mN von Frey filament). **(C)** Nocifensive behaviour of PDE mutants with ~73% (*dunce*^{1}) and ~35% (*dunce*^{ML}) residual cAMP hydrolysis rates (Davis and Kiger, 1981). Data are presented as mean and individual values. Asterisks denote level of significance, ***p ≤ 0.001.

Next, we used calcium imaging to directly test whether CIRL modulates the mechanically-evoked activity of nociceptors. To this end, we monitored calcium signals in C4da neurons labelled with GCaMP6m (Chen et al., 2013) during von Frey filament stimulation as previously reported (Hu et al., 2017). Consistent with the behavioural data describing a CIRL-mediated downregulation of nociceptor function, *Cirl*^{RNAi} significantly enhanced calcium responses to noxious mechanical stimulation (Figure 4; Table 1).

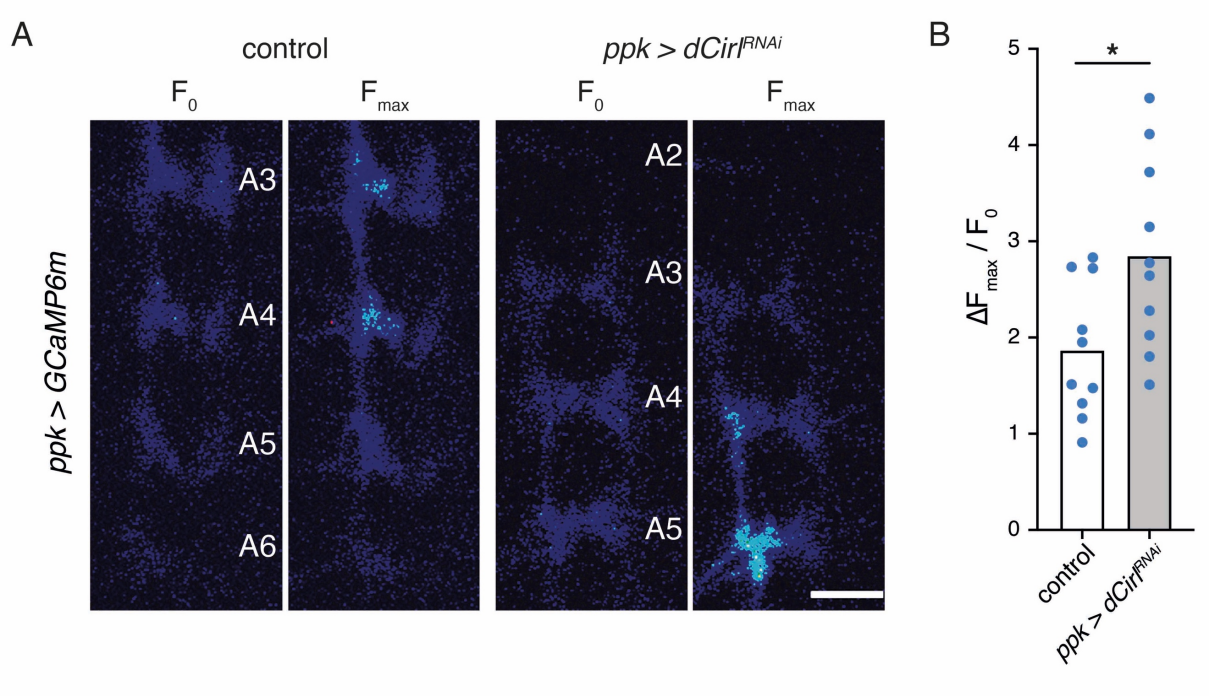

Figure 4. *Cirl* decreases mechanically-evoked calcium currents in nociceptors.
(A) Calcium imaging of C4da axon terminals expressing GCaMP6m (*ppk-GAL4 > UAS-GCaMP6m*) in semi-intact larval preparations. Representative baseline (F_0) and maximum calcium responses (F_{max}) are shown for control and *Cirl*^{RNAi} animals upon von Frey filament stimulation (45 mN). Scale bar, 10 µm. **(B)** Quantification of the calcium signals ($\Delta F_{max}/F_0$) shows that *Cirl*^{RNAi} elevates mechano-nociceptive responses of C4da neurons. Data are presented as mean and individual values. Asterisk denotes level of significance, *p ≤ 0.05.

Having established that CIRL downregulates nociceptor function under physiological conditions, we sought to investigate a pathological setting. The chemotherapeutic agent paclitaxel, employed to treat solid tumours such as ovarian or breast cancer, causes dose-limiting peripheral neuropathy in patients. Similarly, feeding *Drosophila* larvae paclitaxel-supplemented food induces axonal injury and degeneration of C4da neurons (Bhattacharya et al., 2012). Next, we therefore examined nocifensive behaviour in the context of this established neuropathy model. Consistent with chemotherapy-induced allodynia in humans, paclitaxel strongly enhanced nocifensive responses of control larvae (Figure 5A). We observed a comparable effect in *dCirl*^{KO} animals. Overexpressing *Cirl*, in turn, reverted the paclitaxel-induced sensitization of C4da neurons (Figure 5A; Table 1). Thus, CIRL tones down nociceptors in both physiological and neuropathic hyperexcitable states.

Paclitaxel administration causes structural damage to C4da neurons (Bhattacharya et al., 2012). Following paclitaxel treatment (10 µM), we observed dendrite loss in the wild-type background and in nociceptors overexpressing *Cirl* (Figure 5B,C; Table 1). In fact, elevated *Cirl* expression itself reduced the dendritic complexity of C4da neurons. Thus, increasing CIRL protein copy number counteracts the neuropathic hyperexcitability of mechanical nociceptors independently of neuropathy-associated morphological defects. Consistent with the interpretation that modulation of nociceptor physiology by CIRL is not tightly coupled to morphological changes, *dCirl*^{KO} C4da neurons displayed only subtle structural alterations (Figure 5D).

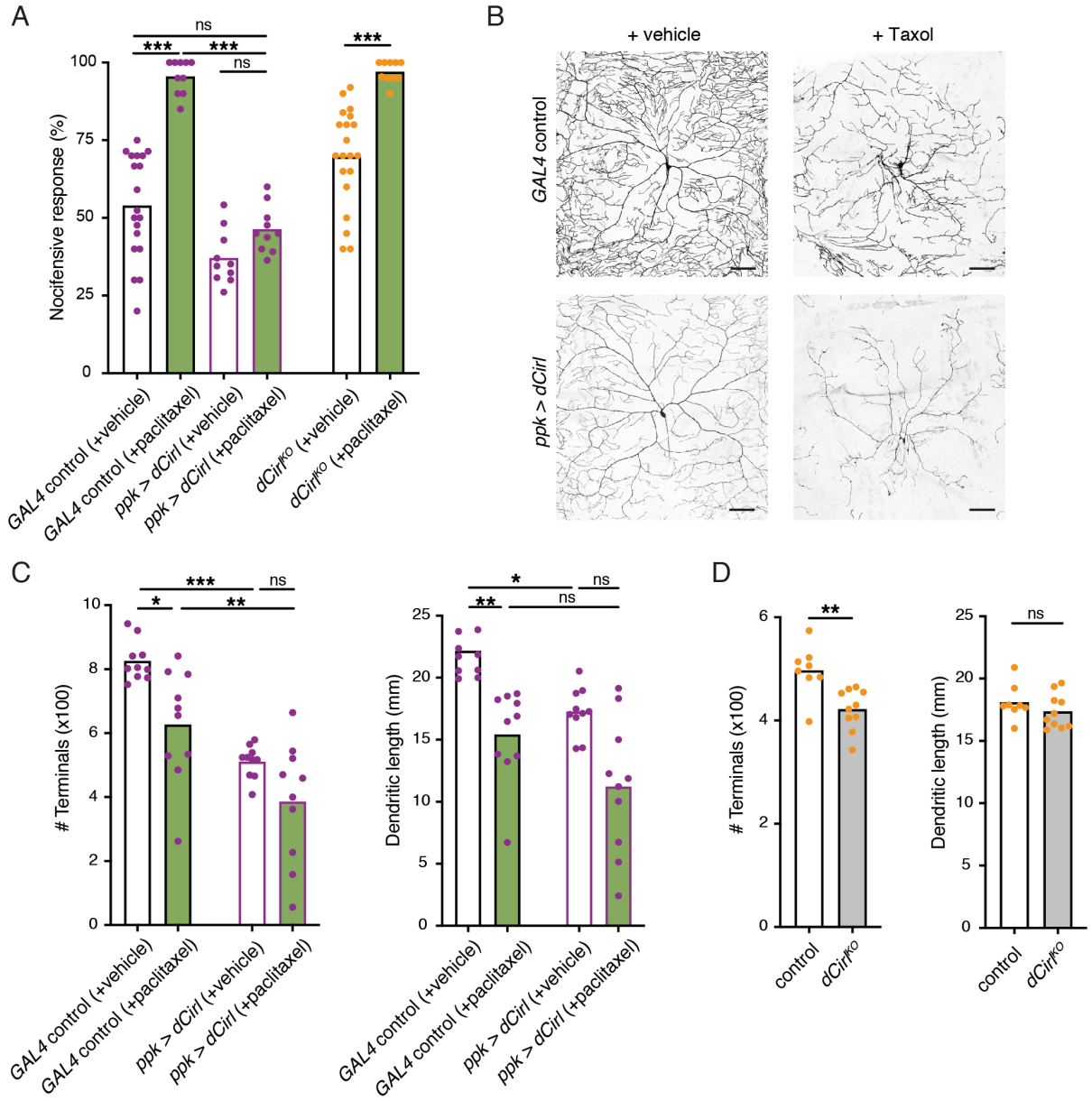

Figure 5. Sensitization of nociceptors through chemotherapy-induced neuropathy.
(A) Increased nocifensive behaviour following paclitaxel treatment (10 µM) is counteracted by overexpressing *Cirl* in nociceptors. **(B)** Example images of C4da neuron morphology upon paclitaxel administration and *Cirl* overexpression. Scale bars, 100 µm. **(C, D)** Morphometric quantification of dendritic complexity of C4da neurons in the different genotypes. Data are presented as mean and individual values. Asterisks denote level of significance, *p ≤ 0.05, **p ≤ 0.01, ***p ≤ 0.001.

Considering the evolutionary conservation of signalling pathways for nociception (Im and Galko, 2012), we next turned to a rodent model of traumatic neuropathic pain: unilateral chronic constriction injury (CCI) of the sciatic nerve (Reinhold et al., 2019). This model resembles paclitaxel-induced neuropathy in the development of thermal hypersensitivity and mechanical allodynia (Sisignano et al., 2016), i.e. a noxious reaction to innocuous stimuli like touch, reaching a maximum after one week (Fig. 6A; Table 1). There are three CIRL proteins in mammals (CIRL1-3 also known as ADGRL1-3 or Lphn1-3) (Langenhan et al., 2016). According to RNA sequencing data from mouse DRG neurons, *Cirl1* and *Cirl3* are expressed in nociceptors (Thakur et al., 2014). We therefore investigated *Cirl1* and *Cirl3* expression in subpopulations of DRG neurons via *in situ* hybridization in the neuropathic context. Interestingly, *Cirl1* mRNA probes described significantly reduced transcript levels in isolectin-B4 (IB4)-positive, non-peptidergic nociceptors one week after CCI (Figure 6B; Table 1). We observed a similar, though statistically insignificant trend in peptidergic nociceptors identified by calcitonin gene-related peptide (CGRP) staining and for *Cirl3* probes (Figure 6C; Table 1). Notably, CCI appeared to neither affect *Cirl1* nor *Cirl3* gene expression in non-nociceptive, large myelinated neurons marked by neurofilament protein NF200. These correlative results are consistent with the *Drosophila* data linking low *Cirl* expression levels to nociceptor sensitization.

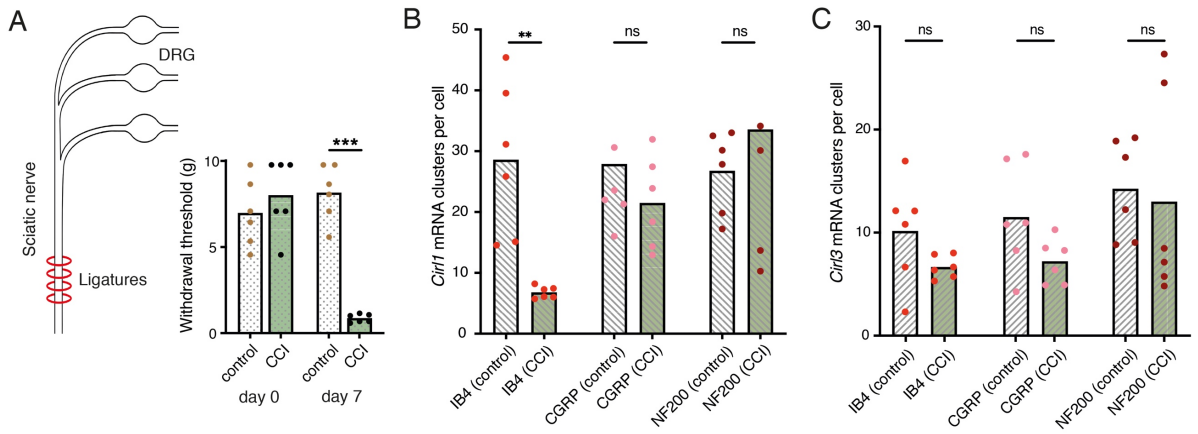

Figure 6. Neuropathy-induced mechanical allodynia correlates with decreased *Cirl1* expression in mammalian non-peptidergic nociceptors.
(**A**) Traumatic injury of the sciatic nerve (CCI, green) in Wistar rats results in mechanical allodynia after one week as measured by von Frey Hairs (paw withdrawal threshold) in comparison to the contralateral side (grey). **(B, C**) Quantification of *Cirl1* (B) and *Cirl3* (C) mRNA levels in subpopulations of rat DRG neurons via *in situ* hybridization (RNAscope). Shown are control conditions (naïve DRGs, grey) and one week after injury (green) following the emergence of allodynia. Data are presented as mean and individual values. Asterisk denotes level of significance, **p ≤ 0.01, ***p ≤ 0.001.

DISCUSSION

The sensations of touch and mechanical pain represent distinct mechanosensory submodalities, which are separated at the initial sites of mechanotransduction. Despite their important roles in health and disease, an understanding of how these mechanistically different transduction processes are carried out at the molecular level is only just beginning to emerge (Delmas et al., 2011; Julius, 2013; Murthy et al., 2017; Szczot et al., 2017; Zhang et al., 2019). In the present study, we provide evidence that CIRL, an evolutionarily conserved aGPCR, reduces nociceptor responses to mechanical insult in *Drosophila* larvae. This modulation operates in the opposite direction to the sensitization of touch sensitive neurons by CIRL (Figure 7) (Scholz et al., 2015, 2017). In both types of mechanosensors, these effects are connected to CIRL-dependent quenching of cAMP levels. The opposing cell physiological outcomes, in turn, likely arise from specific adjustments of different effector proteins. Candidate effectors are mechanotransduction channels or ion channels, which are mechanically-insensitive but influence the rheobase, i.e. the threshold current of the sensory neuron (Boiko et al., 2017).

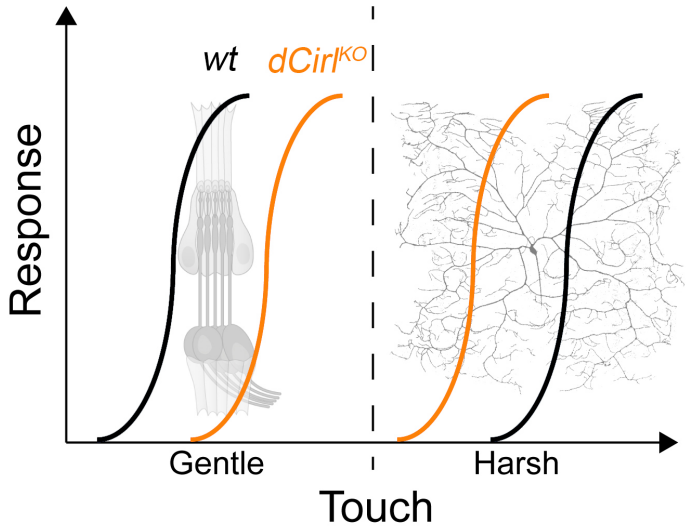

Figure 7. CIRL adjusts mechanosensory submodalities in opposite directions.
Scheme summarizing how the transduction of different levels of mechanical force is bidirectionally modulated by *Drosophila* CIRL. Whereas low threshold mechanosensory neurons (ChOs; gentle touch) are less responsive in *Cirl* mutants, high threshold mechanical nociceptors (C4da neurons; harsh touch) become sensitized.

The TRP (*transient receptor potential*) channel subunits NOMPC (*no receptor potential,* TRPN), NAN (*nanchung*, TRPV), and IAV (*inactive*, TRPV) govern mechanosensation by larval ChO neurons (Effertz et al., 2012; Lehnert et al., 2013; Zhang et al., 2013). The mechanically gated ion channel Piezo, the DEG/ENaC subunit Pickpocket, and the TRPN channel Painless, on the other hand, are required for mechanical nociception in *Drosophila* (Tracey et al., 2003; Zhong et al., 2010; Kim et al., 2012; Gorczyca et al., 2014; Guo et al., 2014; Mauthner et al., 2014). It is therefore conceivable that the receptor potential generated by these different mechanotransducers may be modulated in opposite directions, i.e. decreased in ChO neurons and increased in nociceptors, by cAMP/PKA (protein kinase A)-dependent channel phosphorylation. Matching our results in *Drosophila*, enhanced nociceptor activity in mammals has been linked to elevated cAMP levels. For example, mechanical hyperalgesia during inflammation involves cAMP-modulated HCN channels and sensitization of mammalian Piezo2 via PKA and protein kinase C (PKC) based signalling (Emery et al., 2011; Dubin et al., 2012). Conversely, $G_{i/o}$-coupled receptors, such as opioid, somatostatin, and $GABA_B$ receptors, counteract cAMP-dependent nociceptor sensitization (Yudin and Rohacs, 2018). In addition to this second messenger pathway, $G_{\beta\gamma}$ subunits of $G_{i/o}$-coupled GPCRs can directly

interact with ion channels. Thereby nociceptor signalling can be suppressed via activation of G protein regulated inwardly rectifying K^+ channels (GIRK) or by inhibition of voltage-gated Ca^{2+} channels (Logothetis et al., 1987; Marker et al., 2005; Bourinet et al., 2014). It will be of great interest to investigate whether $G_{i/o}$-protein coupling by CIRL modulates *Drosophila* nociceptors via similar molecular pathways. Recent work has identified a role for CIRL2 and CIRL3 in synapse formation in the mouse hippocampus (Sando et al., 2019). While *Drosophila* CIRL may also shape synaptic connectivity, our results indicate that CIRL modulates the mechanically-evoked activity of nociceptors independently of such an additional function.

Many genes display altered expression in DRG neurons in neuropathy (Lopes et al., 2017). For example, receptors and ion channels involved in sensitization are upregulated, whereas endogenous antinociceptive mechanisms, including opioid receptors and their peptides, are downregulated in certain neuropathy models (Herradon et al., 2008; Hervera et al., 2011). Thus, neuropathy not only enhances pro-nociceptive mechanisms but also decreases endogenous antinociceptive pathways. Our analysis of rodent DRGs indicates that neuropathy-induced allodynia correlates with reduced *Cirl1* expression in IB4-positive non-peptidergic nociceptors (Fang et al., 2006), a class of neurons which have been linked to mechanical inflammatory hypersensitivity (Pinto et al., 2019). It is therefore tempting to speculate that CIRL operates via a conserved antinociceptive mechanism in both invertebrate and mammalian nociceptors to reduce cAMP concentrations. Future work will have to test this hypothesis by examining a direct causal relation between CIRL activation and nociceptor attenuation in the mammalian peripheral nervous system and to explore whether metabotropic mechanosensing by CIRL is a possible target for analgesic therapy. Limited options for treating chronic pain have contributed to the current opioid epidemic (Skolnick and Volkow, 2016). Opioids are powerful analgesics but have severe side effects and lead to addiction mainly through activation of receptors in the central nervous system. There is thus a strong incentive to develop novel peripherally acting pain therapeutics.

Using the experimentally accessible peripheral nervous system of *Drosophila*, we report a new molecular principle underlying the processing of mechanical input. The specificity theory, put forward more than 100 years ago (Sherrington, 1906), defines nociceptors as a functionally distinct subtype of nerve endings, which are specifically tuned to detect harmful, high-intensity stimuli. The results reported in the present study are consistent with this validated concept and identify a physiological mechanism, which contributes to the functional specialization. On the one hand, modulation by CIRL helps set the high activation threshold of mechanical nociceptors, while on the other hand, CIRL lowers the activation threshold of touch sensitive neurons (Figure 7). This bidirectional adjustment moves both submodalities further apart and sharpens the contrast of mechanosensory signals carrying different information.

MATERIALS AND METHODS

Drosophila experiments

Fly stocks

Animals were raised at 25°C on standard cornmeal and molasses medium. The following fly strains were used in this study:

UAS-dCirl^{RNAi} (VDRC#100749): *w*^{1118}*; phiC31{KK108383}v100749* (Dietzl et al., 2007)

w^{1118}*; UAS-bpac/CyOGFP w*$^{-}$ (Stierl et al., 2011)

from (Scholz et al., 2015, 2017):

dCirlp^{GAL4} (LAT84): *w*^{1118}*; dCirl*^{KO} *{w*$^{+mC}$*=pTL464[dCirlp::GAL4]}attP*^{dCirl} *loxP/CyOGFP w*$^{-}$

dCirl^{KO} (LAT26): *w*^{1118}*; dCirl*^{KO} *attP*^{dCirl} *loxP*

dCirl^{Rescue} (LAT163): *w*^{1118}*; dCirl*^{KO} *{w*$^{+mC}$*=pTL370[dCirl]}attP*^{dCirl} *loxP*

20xUAS-dCirl (LAT85): *w*^{1118}*;; {w*$^{+mC}$*=pTL471[20xUAS-IVS-dCirl::3xFlag]}attP2*

dCirl^{KO} *20xUAS-dCirl* (LAT111): *w*^{1118}*; dCirl*^{KO} *attP*^{dCirl} *loxP; {w*$^{+mC}$*=pTL471[20xUAS-IVS-dCirl::3xFlag]}attP2/TM6B, Tb*

from the Bloomington *Drosophila* Stock Center:

BDSC#42748: *w*^{1118}*; UAS-GCaMP6m P{y*$^{+t7.7}$*w*$^{+mC}$*=20xUAS-IVS-GCaMP6m}attP40*

BDSC#35843: *w^{1118};; P{w^{+mC}=ppk-CD4::tdGFP}8/TM6B,Tb*

BDSC#35841: *y^{1} w*; P{w^{+mC}=UAS-CD4::tdTomato}7M1*

BDSC#32078: *w*; P{w^{+mC}=ppk-GAL4.G}2*

BDSC#32079: *w*;; P{w^{+mC}=ppk-GAL4.G}3*

BDSC#6020: *dnc^{1}*

BDSC#43: *f^{36a}*

BDSC#9407: *y^{1} w^{1} dnc^{ML} f^{36a}/FM7a*

Figure 1:

dCirlp^{GAL4}/UAS-CD4::tdTomato; ppk-CD4::tdGFP/+

Figure 2:

control: *dCirl^{Rescue}*

dCirl^{KO}

RNAi control: *UAS-dCirl^{RNAi}/+*

ppk > dCirl^{RNAi}: *ppk-GAL4/UAS-dCirl^{RNAi}*

GAL4 control: *dCirl^{Rescue}/+; ppk-GAL4/+*

dCirl^{KO} ppk > dCirl: *dCirl^{KO}; ppk-GAL4/20xUAS-dCirl*

ppk > dCirl: *ppk-GAL4/20xUAS-dCirl*

Figure 3:

wild-type: *w^{1118}*

ppk > bPAC: *ppk-GAL4/UAS-bpac*

dCirl^{KO} ppk > bPAC: *dCirl^{KO}, UAS-bpac/dCirl^{KO}; ppk-GAL4/+*

control for *dunce^{1}*: Canton-S

control for *dunce^{ML}*: *f^{36a}*

Figure 4:

control: *UAS-GCaMP6m/+; ppk-GAL4/+*

ppk > dCirl^{RNAi}: *UAS-GCaMP6m/UAS-dCirl^{RNAi}; ppk-GAL4/+*

Figure 5:

(A) *GAL4* control: *ppk-GAL4/+*

ppk > dCirl: *ppk-GAL4/20xUAS-dCirl*

$dCirl^{KO}$

(B,C) *GAL4* control: *ppk-GAL4/+; ppk-CD4::tdGFP/+*

ppk > dCirl: *ppk-GAL4/+; ppk-CD4::tdGFP/ 20xUAS-dCirl*

(D) Control: *ppk-Gal4, UAS-CD4::tdTomato*

$dCirl^{KO}$: $dCirl^{KO}$*; ppk-Gal4, UAS-CD4::tdTomato*

Immunohistochemistry

Stainings of the $dCirlp^{GAL4}$- and *ppk*-positive neurons were performed essentially as previously reported (Ehmann et al., 2014). Third instar larvae were dissected in cold PBS, fixed in 4% paraformaldehyde for 10 min at room temperature (RT), and blocked for 30 min in 0.3% PBT (PBS with 0.3% Triton X-100, Sigma-Aldrich) supplemented with 5% normal goat serum (NGS). The preparations were incubated with primary antibodies (diluted in 0.3% PBT with 5% NGS) at 4°C overnight. After rinsing twice and washing 6 x for 10 min with 0.3% PBT, the samples were incubated with secondary antibodies (diluted in 0.3% PBT with 5% NGS) for 120 min at RT. Following two rinsing and 6 x 10 min washing steps with 0.3% PBT, the preparations were immersed in Vectashield (Vector Laboratories) and stored for at least one night at 4°C. The following primary antibodies were used: mouse-α-GFP (1:200; Sigma-Aldrich, SAB4200681; RRID:AB_2827519), rabbit-α-RFP (1:200; antibodies-online, ABIN129578; RRID:AB_10781500). Secondary antibodies: Alexa Fluor-488-conjugated goat-α-mouse (1:250; Invitrogen, A-11001; RRID:AB_2534069) and Cy3-conjugated goat-α-rabbit (1:250; Jackson ImmunoResearch, 111-165-003; RRID:AB_2338006,). Samples were mounted in Vectashield and confocal images (Figure 1) were acquired with a LSM 800 (Zeiss) and a Leica TCS SP5. Intensity and contrast were set using Fiji (Schindelin et al., 2012) and Photoshop CC 2018 (Adobe).

Nociceptor morphometry

For analyses of C4da neuron morphology, staged third instar larvae (96 ± 3 h after egg laying, AEL), raised in density-controlled vials, were mounted in halocarbon oil. Confocal images of photoprotein signals (*ppk-GAL4* > *UAS-CD4::tdGFP* or *UAS-CD4::tdTomato*) were collected with a Zeiss LSM700 laser scanning microscope. Image stacks with a Z step size between 0.5-2 µm were acquired from abdominal segment A5 with a 20×/0.8 objective and quantified with Imaris (Bitplane) using the filament tracer tool.

Nocifensive behaviour

For mechanical nociception assays, wandering third instar larvae were collected in a sylgard covered Petri dish and stimulated with a 40 mN von Frey filament (made from fishing line, 0.22 mm diameter, Caperlan; calibrated with a precision balance). A single noxious mechanical stimulus was rapidly delivered to midabdominal segments (~A4-A6) on the dorsal side of the larva. A positive response was scored if stimulation elicited at least one nocifensive corkscrew body roll. For all behavioural experiments each animal was tested only once. All data were collected from at least seven trials (n, Table 1) each sampling 6-53 larvae.

Calcium imaging

Calcium imaging of C4da axon terminals was performed as previously described (Hu et al., 2017). Briefly, staged third instar larvae (96 ± 3 h AEL) were pinned on a Sylgard (Dow Corning) plate and partially dissected in physiological saline to expose the ventral nerve cord (VNC). C4da neuron axon terminals expressing GCaMP6m were live-imaged by confocal microscopy with a 40× water objective (Olympus FV1000MP) with 3x zoom to image at least 4 segments ensuring the calcium response could be detected. Activation of sensory neurons was achieved by providing a mechanonociceptive cue using a micromanipulator-mounted von Frey filament (45 mN) for stimulation of midabdominal segments (A3–A5). The most robust responses to local von Frey filament stimulation are restricted to a single VNC hemisegment corresponding to the stimulation site on the body wall although the adjacent segment(s) could

also be slightly activated. Baseline (F_0) and relative maximum intensity change (ΔF_{max}) of GCaMP6m fluorescence were analysed.

Optogenetics

Larvae were placed in a drop of water on a Sylgard-coated Petri dish and monitored with a stereomicroscope (Olympus SZX16). After applying blue light (~200 µW/mm^2 at 475 nm) for 3 min, the animals were mechanically stimulated with a von Frey filament (see above). Each larva was scored according to the following criteria. no response: no nocifensive or irregular behaviour during light or upon mechanical stimulation; stimulated rolling: no nocifensive or irregular behaviour during light, corkscrew body roll upon mechanical stimulation; spontaneous bending: head-swinging or bending during light; stimulated rolling: corkscrew body roll during light. For each set of experiments, three larvae were analysed simultaneously and each animal was tested only once. In Table 2, N refers to the number of individuals tested.

Drosophila neuropathy model

DMSO (dimethyl sulfoxide, vehicle, Sigma Aldrich) or paclitaxel (S1150 Absource Diagnostics, dissolved in DMSO) were carefully mixed into the food vials once ~90% of first instar larvae had hatched. This way, paclitaxel treatment (10 µM) occurred after completion of neurogenesis and axonal pathfinding (Bhattacharya et al., 2012).

Rat experiments

Traumatic neuropathy (Chronic constriction injury, CCI)

Animal care and protocols were performed in accordance with international guidelines for the care and use of laboratory animals (EU Directive 2010/63/EU for animal experiments) and were approved by the Government of Unterfranken (protocol numbers 2-733 and 2-264). Humane endpoints and criteria for discontinuation of the experiments with approved score sheets were defined, and the animals were treated accordingly. Animal studies were reported according to the ARRIVE guidelines (McGrath and Lilley, 2015). Male Wistar rats (200-250 g,

Janvier labs, Le Genest-St-Isle, France) were housed in groups of six on dry litter (12 h:12 h light/dark cycle, 21-25 °C, 45-55% humidity) with food and water *ad libitum*. All experiments were performed during the light phase and equal test groups (n =6) were planned**.** Surgery of the Wistar rats was performed under deep isoflurane anaesthesia (1.8 Vol%, fiO2). After skin incision and exposure of the sciatic nerve by blunt preparation, four loose silk ligatures were made (Perma Silk 6.0, Ethicon Inc.) with approximately 1 mm spacing in between (Sauer et al., 2017). After loosely tightening the ligatures, the skin was stitched (Prolene 5.0, Ethicon Inc.). Animals were euthanized with CO_2 at the end of the experiment.

Mechanical nociceptive thresholds

A series of von Frey filaments (Aesthesio set, Ugo Basile) were used to record the withdrawal threshold of the hind paw to identify the mechanical allodynia response (Lux et al., 2019) and touch sensitivity in neuropathy. Filaments were applied to the plantar surface of the hind paw and held for 1–3 s, until they were bent to a 45° angle. Each paw received stimuli with different filament forces, with a 30 s recovery period between each application. The 50% paw withdrawal threshold for von Frey filament responses was determined using Dixon's up and down method (Dixon, 1980).

In situ hybridization and immunohistochemistry

After euthanizing the rats, DRGs were harvested, embedded in Tissue-Tek O.C.T. Compound (Sakura Finetek Europe B.V.), snap frozen in liquid nitrogen, and stored at -80°C. 10 µm thick cryosections were cut at -20°C (CM3050 S Research Cryostat, Leica Biosystems) and the slides were stored at -80°C until further use. For fixation, tissue sections were placed in precooled 4% PFA in DEPC (diethyl pyrocarbonate)-treated distilled water. Following washing steps with DEPC-treated reagents, probes for rat ADGRL1 and ADGRL3 (tagged with Cy3 and Cy5, respectively) were added for the RNAscope Fluorescent Multiplex Assay (Advanced Cell Diagnostics, Inc.), which was performed according to the manufacturer's instructions (document 320293-USM). After 15 min of incubation at 4°C the samples were dehydrated in

ethanol at RT (50%, 70%, 100%, 100%; 5 min each). Hydrophobic barriers measuring approximately the same area, were drawn around the tissue sections and allowed to dry completely. Afterwards, each section was incubated with two drops of RNAscope Protease IV reagent (15 min at RT). Following the RNAscope assay, samples were washed, blocked with 10% donkey serum in PBS (1 h at RT), and counterstained with neuronal markers (diluted in 10% donkey serum in PBS and added for two nights at 4°C). Non peptidergic nociceptors: isolectin B4 (IB4)-FITC conjugate (1:200, Sigma-Aldrich, L2895); large myelinated mechanosensors and proprioceptors: rabbit anti-NF200 (1:200, Sigma-Aldrich, RRID:AB_477272); peptidergic nociceptors: mouse anti-CGRP (1:150, Abcam, RRID:AB_1658411). Following incubation, the sections were washed and secondary antibodies were added (diluted in PBS and incubated for 1 h at RT). For CGRP: donkey anti-mouse AlexaFluor488 (1:1000, Life Technologies, RRID:AB_141607), for NF200: donkey anti-rabbit AlexaFluor488 (1:1000, Life Technologies, RRID:AB_141708). After washing, the slides were mounted in Vectashield, dried for 15 min at RT, and stored at 4°C until imaging (<24 h). All images were acquired in one session by confocal microscopy (Olympus FV1000) with a 20×/0.75 objective (Olympus UPlan SAPO) using the same parameters for z-stacks (1 µm step size) of Cy3 and Cy5 channels.

Image Evaluation

Images were processed with Fiji (Schindelin et al., 2012) by scientists blinded to the test groups. The markers of neuronal subpopulations were used to identify complete and distinguishable cells as regions of interest (ROIs) for further analysis. Thresholds were applied to maximal projections of confocal z-stacks for Cy3 (grey value 1200) and Cy5 (grey value 1150) signals. Elements between 3 and 22 pixels in size, defined as mRNA clusters, were quantified for each channel following background subtraction. An independent approach based on computational image evaluation gave comparable results (data not shown). Here, a convolutional neural network (DeepFLaSh) (Segebarth et al., 2018) was trained with six

images for each neuronal marker (NF200, IB4, CGRP) and then used to identify Cy3 and Cy5 clusters.

Statistics

Data were analyzed with Prism 8.2 (GraphPad). Group means were compared by an unpaired two- tailed t test, unless the assumption of normal sample distribution was violated, in which case group means were compared by a nonparametric Mann-Whitney rank sum test. To compare more than two groups an ordinary one-way ANOVA with Tukey correction (normal distribution) or a Kruskal-Wallis test (not normally distributed) were used.

ACKNOWLEDGEMENTS

We thank R. Blum for help with the computational image analysis of DRGs, and N. Naumann and B. Goettgens for technical assistance. This work was supported by grants from the Deutsche Forschungsgemeinschaft to M.S. (PA3241/2-1), R.J.K. (FOR 2149/P03, TRR 166/B04, KI1460/4-1, KI1460/5-1), P.S. (SPP 1926/SO1337/2-2, SO1337/4-1), and T.L. (FOR 2149/P01 and P03, TRR 166/C03, LA2861/7-1). Stocks obtained from the Bloomington *Drosophila* Stock Center (NIH P40OD018537) and the Vienna *Drosophila* Resource Center (Dietzl et al., 2007) were used in this study. The authors declare no competing financial interests.

REFERENCES

Abraira VE, Ginty DD (2013) The sensory neurons of touch. Neuron 79:618–639.

Basbaum AI, Bautista DM, Scherrer G, Julius D (2009) Cellular and molecular mechanisms of pain. Cell 139:267–284.

Bhattacharya MRC, Gerdts J, Naylor S a., Royse EX, Ebstein SY, Sasaki Y, Milbrandt J, DiAntonio a. (2012) A model of toxic neuropathy in *Drosophila* reveals a role for

MORN4 in promoting axonal degeneration. J Neurosci 32:5054–5061.

Bodmer R, Jan YN (1987) Morphological differentiation of the embryonic peripheral neurons in *Drosophila*. Roux's Arch Dev Biol 196:69–77.

Boiko N, Medrano G, Montano E, Jiang N, Williams CR, Madungwe NB, Bopassa JC, Kim CC, Parrish JZ, Hargreaves KM, Stockand JD, Eaton BA (2017) TrpA1 activation in peripheral sensory neurons underlies the ionic basis of pain hypersensitivity in response to vinca alkaloids. PLoS One 12:e0186888.

Bourinet E, Altier C, Hildebrand ME, Trang T, Salter MW, Zamponi GW (2014) Calcium-permeable ion channels in pain signaling. Physiol Rev 94:81–140.

Brand AH, Perrimon N (1993) Targeted gene expression as a means of altering cell fates and generating dominant phenotypes. Development 118:401–415.

Chatzigeorgiou M, Yoo S, Watson JD, Lee WH, Spencer WC, Kindt KS, Hwang SW, Miller DM, Treinin M, Driscoll M, Schafer WR (2010) Specific roles for DEG/ENaC and TRP channels in touch and thermosensation in *C. elegans* nociceptors. Nat Neurosci 13:861–868.

Chen TW, Wardill TJ, Sun Y, Pulver SR, Renninger SL, Baohan A, Schreiter ER, Kerr RA, Orger MB, Jayaraman V, Looger LL, Svoboda K, Kim DS (2013) Ultrasensitive fluorescent proteins for imaging neuronal activity. Nature 499:295–300.

Davis RL, Kiger JA (1981) Dunce mutants of *Drosophila melanogaster*: mutants defective in the cyclic AMP phosphodiesterase enzyme system. J Cell Biol 90:101-107.

Delmas P, Hao J, Rodat-Despoix L (2011) Molecular mechanisms of mechanotransduction in mammalian sensory neurons. Nat Rev Neurosci 12:139–153.

Dietzl G, Chen D, Schnorrer F, Su KC, Barinova Y, Fellner M, Gasser B, Kinsey K, Oppel S, Scheiblauer S, Couto A, Marra V, Keleman K, Dickson BJ (2007) A genome-wide transgenic RNAi library for conditional gene inactivation in *Drosophila*. Nature 448:151–156.

Dixon WJ (1980) Efficient analysis of experimental observations. Annu Rev Pharmacol Toxicol 20:441–462.

Dubin AE, Schmidt M, Mathur J, Petrus MJ, Xiao B, Coste B (2012) Inflammatory signals enhance piezo2-mediated mechanosensitive currents. Cell Rep 2:511–517.

Duffy JB (2002) GAL4 system in *Drosophila*: a fly geneticist's Swiss army knife. Genesis 34:1–15.

Effertz T, Nadrowski B, Piepenbrock D, Albert JT, Göpfert MC (2012) Direct gating and mechanical integrity of *Drosophila* auditory transducers require TRPN1. Nat Neurosci 15:1198–1200.

Ehmann N, van de Linde S, Alon A, Ljaschenko D, Keung XZ, Holm T, Rings A, DiAntonio A, Hallermann S, Ashery U, Heckmann M, Sauer M, Kittel RJ (2014) Quantitative super-resolution imaging of Bruchpilot distinguishes active zone states. Nat Commun 5:4650.

Emery EC, Young GT, Berrocoso EM, Chen L, McNaughton PA (2011) HCN2 ion channels play a central role in inflammatory and neuropathic pain. Science 333:1462–1466.

Fang X, Djouhri L, McMullan S, Berry C, Waxman SG, Okuse K, Lawson SN (2006) Intense isolectin-B4 binding in rat dorsal root ganglion neurons distinguishes C-fiber nociceptors with broad action potentials and high Nav1.9 expression. J Neurosci 26:7281–7292.

Ghysen A, Dambly-Chaudière C, Aceves E, Jan LY, Jan YN (1986) Sensory neurons and peripheral pathways in *Drosophila* embryos. Roux Arch Dev Biol 195:281–289.

Gorczyca DA, Younger S, Meltzer S, Kim SE, Cheng L, Song W, Lee HY, Jan LY, Jan YN (2014) Identification of Ppk26, a DEG/ENaC channel functioning with Ppk1 in a mutually dependent manner to guide locomotion behavior in *Drosophila*. Cell Rep 9:1446–1458.

Griffith LC, Budnik V (2006) Plasticity and second messengers during synapse development. Int Rev Neurobiol 75:237–265.

Grueber WB, Jan LY, Jan YN (2002) Tiling of the *Drosophila* epidermis by multidendritic sensory neurons. Development 129:2867–2878.

Grueber WB, Ye B, Moore AW, Jan LY, Jan YN (2003) Dendrites of distinct classes of *Drosophila* sensory neurons show different capacities for homotypic repulsion. Curr Biol 13:618–626.

Guo Y, Wang Y, Wang Q, Wang Z (2014) The role of PPK26 in *Drosophila* larval mechanical

nociception. Cell Rep 9:1183–1190.

Hamann J et al. (2015) International union of basic and clinical pharmacology. XCIV. adhesion G protein-coupled receptors. Pharmacol Rev 67:338–367.

Han C, Jan LY, Jan Y-N (2011) Enhancer-driven membrane markers for analysis of nonautonomous mechanisms reveal neuron-glia interactions in *Drosophila*. Proc Natl Acad Sci U S A 108:9673–9678.

Herradon G, Ezquerra L, Nguyen T, Wang C, Siso A, Franklin B, Dilorenzo L, Rossenfeld J, Silos-Santiago I, Alguacil LF (2008) Noradrenergic and opioidergic alterations in neuropathy in different rat strains. Neurosci Lett 438:186–189.

Hervera A, Negrete R, Leánez S, Martín-Campos JM, Pol O (2011) Peripheral effects of morphine and expression of μ-opioid receptors in the dorsal root ganglia during neuropathic pain: Nitric oxide signaling. Mol Pain 7:25.

Hoffman BD, Grashoff C, Schwartz MA (2011) Dynamic molecular processes mediate cellular mechanotransduction. Nature 475:316–323.

Hu C, Petersen M, Hoyer N, Spitzweck B, Tenedini F, Wang D, Gruschka A, Burchardt LS, Szpotowicz E, Schweizer M, Guntur AR, Yang CH, Soba P (2017) Sensory integration and neuromodulatory feedback facilitate *Drosophila* mechanonociceptive behavior. Nat Neurosci 20:1085–1095.

Im SH, Galko MJ (2012) Pokes, sunburn, and hot sauce: *Drosophila* as an emerging model for the biology of nociception. Dev Dyn 241:16–26.

Julius D (2013) TRP channels and pain. Annu Rev Cell Dev Biol 29:355–384.

Kernan MJ (2007) Mechanotransduction and auditory transduction in *Drosophila*. Pflugers Arch Eur J Physiol 454:703–720.

Kim MJ, Johnson WA (2014) ROS-mediated activation of *Drosophila* larval nociceptor neurons by UVC irradiation. BMC Neurosci 15:14.

Kim SE, Coste B, Chadha A, Cook B, Patapoutian A (2012) The role of *Drosophila* Piezo in mechanical nociception. Nature 483:209–212.

Langenhan T, Piao X, Monk KR (2016) Adhesion G protein-coupled receptors in nervous

system development and disease. Nat Rev Neurosci 17:550–561.

Lehnert BP, Baker AE, Gaudry Q, Chiang AS, Wilson RI (2013) Distinct roles of TRP channels in auditory transduction and amplification in *Drosophila*. Neuron 77:115–128.

Liebscher I, Schön J, Petersen SC, Fischer L, Auerbach N, Demberg LM, Mogha A, Cöster M, Simon KU, Rothemund S, Monk KR, Schöneberg T (2014) A tethered agonist within the ectodomain activates the adhesion G protein-coupled receptors GPR126 and GPR133. Cell Rep 9:2018–2026.

Logothetis DE, Kurachi Y, Galper J, Neer EJ, Clapham DE (1987) The βγ subunits of GTP-binding proteins activate the muscarinic K^+ channel in heart. Nature 325:321–326.

Lopes DM, Malek N, Edye M, Jager SB, McMurray S, McMahon SB, Denk F (2017) Sex differences in peripheral not central immune responses to pain-inducing injury. Sci Rep 7:16460.

Lux TJ, Hu X, Ben-Kraiem A, Blum R, Chen JTC, Rittner HL (2019) Regional differences in tight junction protein expression in the blood-DRG barrier and their alterations after nerve traumatic Injury in rats. Int J Mol Sci 21:270.

Marker CL, Luján R, Loh HH, Wickman K (2005) Spinal G-protein-gated potassium channels contribute in a dose-dependent manner to the analgesic effect of μ- and δ-but not κ-opioids. J Neurosci 25:3551–3559.

Mauthner SE, Hwang RY, Lewis AH, Xiao Q, Tsubouchi A, Wang Y, Honjo K, Skene JHP, Grandl J, Tracey WD (2014) Balboa binds to pickpocket in vivo and is required for mechanical nociception in *Drosophila* larvae. Curr Biol 24:2920–2925.

McGlone F, Wessberg J, Olausson H (2014) Discriminative and affective touch: sensing and feeling. Neuron 82:737–755.

McGrath JC, Lilley E (2015) Implementing guidelines on reporting research using animals (ARRIVE etc.): new requirements for publication in BJP. Br J Pharmacol 172:3189–3193.

Mederos y Schnitzler M, Storch U, Meibers S, Nurwakagari P, Breit A, Essin K, Gollasch M, Gudermann T (2008) Gq-coupled receptors as mechanosensors mediating myogenic

vasoconstriction. EMBO J 27:3092–3103.

Murthy SE, Dubin AE, Patapoutian A (2017) Piezos thrive under pressure: mechanically activated ion channels in health and disease. Nat Rev Mol Cell Biol 18:771–783.

Pinto LG, Souza GR, Kusuda R, Lopes AH, Sant'Anna MB, Cunha FQ, Ferreira SH, Cunha TM (2019) Non-peptidergic nociceptive neurons are essential for mechanical inflammatory hypersensitivity in mice. Mol Neurobiol 56:5715–5728.

Price MP, McIlwrath SL, Xie J, Cheng C, Qiao J, Tarr DE, Sluka KA, Brennan TJ, Lewin GR, Welsh MJ (2001) The DRASIC cation channel contributes to the detection of cutaneous touch and acid stimuli in mice. Neuron 32:1071–1083.

Reinhold A-K, Yang S, Chen JT-C, Hu L, Sauer R-S, Krug SM, Mambretti EM, Fromm M, Brack A, Rittner HL (2019) Tissue plasminogen activator and neuropathy open the blood-nerve barrier with upregulation of microRNA-155-5p in male rats. Biochim Biophys Acta - Mol Basis Dis 1865:1160–1169.

Sando R, Jiang X, Südhof TC (2019) Latrophilin GPCRs direct synapse specificity by coincident binding of FLRTs and teneurins. Science 363:7969.

Sauer RS, Kirchner J, Yang S, Hu L, Leinders M, Sommer C, Brack A, Rittner HL (2017) Blood–spinal cord barrier breakdown and pericyte deficiency in peripheral neuropathy. Ann N Y Acad Sci 1405:71–88.

Schindelin J, Arganda-Carreras I, Frise E, Kaynig V, Longair M, Pietzsch T, Preibisch S, Rueden C, Saalfeld S, Schmid B, Tinevez J-Y, White DJ, Hartenstein V, Eliceiri K, Tomancak P, Cardona A (2012) Fiji: an open-source platform for biological-image analysis. Nat Methods 9:676–682.

Scholz N, Gehring J, Guan C, Ljaschenko D, Fischer R, Lakshmanan V, Kittel RJ, Langenhan T (2015) The adhesion GPCR Latrophilin/CIRL shapes mechanosensation. Cell Rep 11:866–874.

Scholz N, Guan C, Nieberler M, Grotemeyer A, Maiellaro I, Gao S, Beck S, Pawlak M, Sauer M, Asan E, Rothemund S, Winkler J, Nagel G, Langenhan T, Kittel RJ, Scho R (2017) Mechano-dependent signaling by Latrophilin / CIRL quenches cAMP in proprioceptive

neurons. Elife 6:e28360.

Scholz N, Monk KR, Kittel RJ, Langenhan T (2016) Adhesion GPCRs as a putative class of metabotropic mechanosensors. In: Adhesion G Protein-coupled Receptors: Molecular, Physiological and Pharmacological Principles in Health and Disease (Langenhan T, Schöneberg T, eds). Handb Exp Pharmacol 234:221–247, Springer, Cham.

Segebarth D, Griebel M, Duerr A, Collenberg CR von, Martin C, Fiedler D, Comeras LB, Sah A, Stein N, Gupta R, Sasi M, Lange MD, Tasan RO, Singewald N, Pape H-C, Sendtner M, Flath CM, Blum R (2018) DeepFLaSh, a deep learning pipeline for segmentation of fluorescent labels in microscopy images. bioRxiv:473199.

Sherrington CS (1906) The integrative action of the nervous system. Scribner and Sons, New York.

Sisignano M et al. (2016) Targeting CYP2J to reduce paclitaxel-induced peripheral neuropathic pain. Proc Natl Acad Sci U S A 113:12544–12549.

Skolnick P, Volkow ND (2016) Re-energizing the development of pain therapeutics in light of the opioid epidemic. Neuron 92:294–297.

Stierl M, Stumpf P, Udwari D, Gueta R, Hagedorn R, Losi A, Gärtner W, Petereit L, Efetova M, Schwarzel M, Oertner TG, Nagel G, Hegemann P (2011) Light modulation of cellular cAMP by a small bacterial photoactivated adenylyl cyclase, bPAC, of the soil bacterium Beggiatoa. J Biol Chem 286:1181–1188.

Stoveken HM, Hajduczok AG, Xu L, Tall GG (2015) Adhesion G protein-coupled receptors are activated by exposure of a cryptic tethered agonist. Proc Natl Acad Sci U S A 112:6194–6199.

Szczot M, Pogorzala LA, Solinski HJ, Young L, Yee P, Le Pichon CE, Chesler AT, Hoon MA (2017) Cell-Type-Specific Splicing of Piezo2 Regulates Mechanotransduction. Cell Rep 21:2760–2771.

Thakur M, Crow M, Richards N, Davey GI, Levine E, Kelleher JH, Agley CC, Denk F, Harridge SD, McMahon SB (2014) Defining the nociceptor transcriptome. Front Mol Neurosci 7:87.

Tracey WD, Wilson RI, Laurent G, Benzer S (2003) painless, a *Drosophila* gene essential for nociception. Cell 113:261–273.

Xiang Y, Yuan Q, Vogt N, Looger LL, Jan LY, Jan YN (2010) Light-avoidance-mediating photoreceptors tile the *Drosophila* larval body wall. Nature 468:921–926.

Yudin Y, Rohacs T (2018) Inhibitory $G_{i/O}$-coupled receptors in somatosensory neurons: potential therapeutic targets for novel analgesics. Mol Pain 14.

Zhang M, Wang Y, Geng J, Zhou S, Xiao B (2019) Mechanically activated Piezo channels mediate touch and suppress acute mechanical pain response in mice. Cell Rep 26:1419-1431.e4.

Zhang W, Yan Z, Jan LY, Jan YN (2013) Sound response mediated by the TRP channels NOMPC, NANCHUNG, and INACTIVE in chordotonal organs of *Drosophila* larvae. Proc Natl Acad Sci 110:13612–13617.

Zhong L, Bellemer A, Yan H, Honjo K, Robertson J, Hwang RY, Pitt GS, Tracey WD (2012) Thermosensory and nonthermosensory isoforms of *Drosophila melanogaster* TRPA1 reveal heat-sensor domains of a thermo TRP channel. Cell Rep 1:43–55.

Zhong L, Hwang RY, Tracey WD (2010) Pickpocket is a DEG/ENaC protein required for mechanical nociception in *Drosophila* larvae. Curr Biol 20:429–434.

FIGURE LEGENDS

Figure 1. *Drosophila Cirl* is expressed in proprioceptors and nociceptors.
(A) The *Cirl* promoter drives *Tomato* photoprotein expression (magenta; *dCirlp^{GAL4}* > *UAS-CD4::tdTomato*) in type 1 larval pentascolopidial ChO (lch5) neurons and type 2 C4da nociceptors, identified by a *GFP-ppk* promoter fusion (green; *ppk-CD4::tdGFP*). Magnified view of **(B)** C4da and **(C)** ChO neurons. Shown are immunohistochemical stainings against the photoproteins. Scale bars (A) 20 µm, (B,C) 10 µm.

Figure 2. *Cirl* reduces nocifensive behaviour.

(A) Characteristic nocifensive 'corkscrew' roll of larvae upon mechanical stimulation with a von Frey filament (40 mN force). **(B)** Quantification of nocifensive behaviour in different genotypes. Increased nocifensive responses were observed in *dCirl*^{KO} and upon nociceptor-specific expression of an RNAi construct (*ppk-GAL4* > *UAS-dCirl*^{RNAi}). *Cirl* re-expression rescued the null mutant (*dCirl*^{KO} *ppk-GAL4* > *UAS-dCirl*) and *Cirl* overexpression (*ppk-GAL4* > *UAS-dCirl*) reduced nocifensive responses. Raising animals at a higher temperature (29°C vs. 25°C) increases *UAS/GAL4*-dependent transgene expression (Duffy, 2002). Data are presented as mean and individual values (lower bar plot) and as the difference between means with 95% confidence intervals (upper dot plot). Asterisks denote level of significance, *p ≤ 0.05, **p ≤ 0.01, ***p ≤ 0.001.

Figure 3. Potentiation of nociceptor function by cAMP.

(A) Schematic illustration of cAMP production by bPAC. **(B)** Optogenetic assay. Stimulated and spontaneous nocifensive responses can be promoted and elicited, respectively, by bPAC activation in C4da neurons (blue labels, photostimulation). Larval behaviour was observed during 3 min illumination (~200 µW/mm^2 at 475 nm) followed by mechanical stimulation (40 mN von Frey filament). **(C)** Nocifensive behaviour of PDE mutants with ~73% (*dunce*^{1}) and ~35% (*dunce*^{ML}) residual cAMP hydrolysis rates (Davis and Kiger, 1981). Data are presented as mean and individual values. Asterisks denote level of significance, ***p ≤ 0.001.

Figure 4. *Cirl* decreases mechanically-evoked calcium currents in nociceptors.

(A) Calcium imaging of C4da axon terminals expressing GCaMP6m (*ppk-GAL4* > *UAS-GCaMP6m*) in semi-intact larval preparations. Representative baseline (F_0) and maximum calcium responses (F_{max}) are shown for control and *Cirl*^{RNAi} animals upon von Frey filament stimulation (45 mN). Scale bar, 10 µm. **(B)** Quantification of the calcium signals ($\Delta F_{max}/F_0$) shows that *Cirl*^{RNAi} elevates mechano-nociceptive responses of C4da neurons. Data are presented as mean and individual values. Asterisk denotes level of significance, *p ≤ 0.05.

Figure 5. Sensitization of nociceptors through chemotherapy-induced neuropathy.

(A) Increased nocifensive behaviour following paclitaxel treatment (10 µM) is counteracted by overexpressing *Cirl* in nociceptors. **(B)** Example images of C4da neuron morphology upon paclitaxel administration and *Cirl* overexpression. Scale bars, 100 µm. **(C, D)** Morphometric quantification of dendritic complexity of C4da neurons in the different genotypes. Data are presented as mean and individual values. Asterisks denote level of significance, *p ≤ 0.05, **p ≤ 0.01, ***p ≤ 0.001.

Figure 6. Neuropathy-induced mechanical allodynia correlates with decreased *Cirl1* expression in mammalian non-peptidergic nociceptors.

(**A**) Traumatic injury of the sciatic nerve (CCI, green) in Wistar rats results in mechanical allodynia after one week as measured by von Frey Hairs (paw withdrawal threshold) in comparison to the contralateral side (grey). **(B, C**) Quantification of *Cirl1* (B) and *Cirl3* (C) mRNA levels in subpopulations of rat DRG neurons via *in situ* hybridization (RNAscope). Shown are control conditions (naïve DRGs, grey) and one week after injury (green) following the emergence of allodynia. Data are presented as mean and individual values. Asterisk denotes level of significance, **p ≤ 0.01, ***p ≤ 0.001.

Figure 7. CIRL adjusts mechanosensory submodalities in opposite directions.

Scheme summarizing how the transduction of different levels of mechanical force is bidirectionally modulated by *Drosophila* CIRL. Whereas low threshold mechanosensory neurons (ChOs; gentle touch) are less responsive in *Cirl* mutants, high threshold mechanical nociceptors (C4da neurons; harsh touch) become sensitized.

1 **Table 1**

Figure	Genotype	mean	SEM	n	P-value	test
Fig. 2B	control	53.34	1.458	7	p<0.0001	unpaired t-test
	dCirl^{KO}	75.37	2.676	10		
	RNAi control	54.23	3.279	8	p=0.0169	one-way ANOVA, Tukey correction
	ppk > dCirl^{RNAi}	68.08	2.052	10		
	GAL4 control	53.67	3.211	14		one-way ANOVA, Tukey correction
	KO ppk > dCirl	45.7	3.627	10	p=0.3345 (*GAL4* control)	
	ppk > dCirl	37.12	2.778	10	p=0.0023 (*GAL4* control)	
	ppk > dCirl (29°C)	28.67	3.125	10	p<0.0001 (*GAL4* control)	
Fig. 3C	control (Canton-S)	44	3.712	10	p<0.0001	Mann-Whitney
	dunce^{1}	72	1.106	12		
	control (*f*^{36a})	50.5	3.343	10	p<0.0001	unpaired t-test
	dunce^{ML}	79.58	0.965	12		
Fig. 4B	control	1.869	0.2226	10	p=0.021	unpaired t-test
	ppk > dCirl^{RNAi}	2.85	0.3176	10		
Fig. 5A	*GAL4* control (+vehicle)	53.96	3.831	19	p>0.9999 (*ppk>dCirl* +Taxol)	Kruskal-Wallis test
	GAL4 control (+Taxol)	95.5	1.74	10	p=0.0002 (*GAL4* control +vehicle)	
	ppk > dCirl (+vehicle)	37.12	2.778	10	p>0.9999 (*ppk>dCirl* +Taxol)	
	ppk > dCirl (+Taxol)	46.34	2.374	10	p<0.0001 (*GAL4* control +Taxol)	
	dCirl^{KO} (+vehicle)	69.68	3.54	20	p<0.0001	Mann-Whitney
	dCirl^{KO} (+Taxol)	97.05	1.097	10		
Fig. 5C	*GAL4* control (+vehicle)	8.256	0.1985	10	p=0.0117 (*GAL4* control +Taxol)	Kruskal-Wallis test
	GAL4 control (+Taxol)	6.27	0.5574	10	p=0.0017 (*ppk>dCirl* +Taxol)	
	ppk > dCirl (+vehicle)	5.108	0.1603	10	p<0.0001 (*GAL4* control +vehicle)	
	ppk > dCirl (+Taxol)	3.861	0.5961	10	p=0.1848 (*ppk>dCirl* +vehicle)	
	GAL4 control (+vehicle)	22.17	0.7015	10	p=0.0014 (*GAL4* control +Taxol)	one-way ANOVA, Tukey correction
	GAL4 control (+Taxol)	15.42	1.174	10	p>0.9999 (ppk>dCirl +Taxol)	
	ppk > dCirl (+vehicle)	17.26	0.6091	10	p=0.0296 (*GAL4* control +vehicle)	
	ppk > dCirl (+Taxol)	11.22	1.716	10	p=0.2557 (*ppk>dCirl* +vehicle)	
Fig. 5D	control	4.971	0.1747	8	p=0.0025	unpaired t-test
	dCirl^{KO}	4.219	0.1255	10		
	control	18.11	0.5029	8	p=0.2829	unpaired t-test

	dCirl^{KO}	17.37	0.4384	10		
Fig. 6A	control day 0	6.972	0.8056	6	p=0.4062	unpaired t-test
	CCI day 0	8.003	0.8755	6		
	control day 7	8.152	0.6647	6	p<0.0001	
	CCI day 7	0.861	0.0982	6		
Fig. 6B	IB4 (control)	28.6	5.148	6	p=0.0018	unpaired t-test
	IB4 (CCI)	6.791	0.4034	6		
	CGRP (control)	27.89	5.529	6	p=0.3358	
	CGRP (CCI)	21.49	3.078	6		
	NF200 (control)	26.76	2.737	6	p=0.45	
	NF200 (CCI)	33.57	8.216	6		
Fig. 6C	IB4 (control)	10.16	2.065	6	p=0.1293	unpaired t-test
	IB4 (CCI)	6.662	0.4542	6		
	CGRP (control)	11.5	2.103	6	p=0.0895	
	CGRP (CCI)	7.212	0.8851	6		
	NF200 (control)	14.25	1.965	6	p=0.3939	Mann-Whitney
	NF200 (CCI)	13	4.133	6		

Table 2

Figure	Genotype	mean 0	mean 1	mean 2	mean 3	N
Fig. 3B	wild-type (dark)	47.29	52.71	0.00	0.00	203
	wild-type (light)	48.00	52.00	0.00	0.00	200
	ppk > bPAC (dark)	31.25	53.13	15.63	0.00	96
	ppk > bPAC (light)	5.13	56.41	28.21	10.26	39
	KO ppk > bPAC (dark)	0.00	70.00	26.67	3.33	30
	KO ppk > bPAC (light)	0.00	58.06	12.90	29.03	31

0: no response, 1: stimulated rolling, 2: spontaneous bending, 3: spontaneous rolling